ESR Study of MMA Batch Emulsion Polymerization in Real Time: Effects of Particle Size

H.-Y. Parker, D. G. Westmoreland, and H.-R. Chang*,†

Rohm and Haas Company, Spring House, Pennsylvania 19477

Received November 3, 1995; Revised Manuscript Received April 25, 1996[⊗]

ABSTRACT: An experimental methodology has been developed which combines a continuous-flow system and an electron spin resonance time sweep experiment to study the batch emulsion polymerization of methyl methacrylate (MMA). This system allows essentially continuous monitoring of the propagating free-radical concentration during the reaction. The polymerization was initiated by a redox initiator system at a relatively low temperature (45 °C). This technique has been used to study the effect of varying latex particle size on polymerization kinetics. This study demonstrates that latex particle size has a significant effect on the PMMA propagating radical concentration profile, which is hypothesized to be due to changing the balance of the radical termination reactions. This study also provides evidence for an inhomogeneous distribution of the propagating PMMA radicals in the latex particle. The magnitude of the proposed inhomogeneity depends on the size of the particles.

Introduction

Latex particle size is a very important parameter for emulsion polymerization. This is not only because of the close linkage between the particle size and final properties of many products based on latex polymers but also because it has become a more recognized factor which can strongly influence the polymerization kinetics in the heterogeneous system. A long time ago, it was found that in very small particle size emulsion polymerization, and in the case of miniemulsion polymerization of styrene, extremely high molecular weight was achieved.[1] This was believed to be a result of a "zero−one" condition in which particles contain either one or no propagating radicals, and the average number of radicals per particle is 0.5. Recently, independent research groups have demonstrated that varying latex particle size changes the rate of polymerization.[2,3] These studies indicated that for batch polymerization of methyl methacrylate (MMA) in either macro- or miniemulsion, the overall rate of monomer conversion decreases as the particle size increases.

Recently, a considerable advance beyond the conventional emulsion/bulk polymerization theory was made by several groups.[4−8] Their work concluded that many kinetic parameters, such as rate coefficients of propagation and termination, are chain-length dependent rather than constant, because diffusion of the propagating radicals and even monomers could become rate limiting. This conclusion led to the recognition of inhomogeneous polymerization inside the latex particle, though different factors that may cause the inhomogeneity had been proposed. Inhomogeneities in latex particles have been studied by both theoretical simulation and small-angle neutron scattering.[9−14] Since particle size directly relates to the diffusion distance of propagating radical species and monomers, it is important to investigate how particle size affects the development of particle inhomogeneity during emulsion polymerization. We have carried out an in-depth study of the propagating radicals during batch emulsion polymerization of MMA at various latex particle sizes with the goal of better understanding how particle size affects kinetics and radical distribution.

One of the most powerful tools for the study of free radicals during polymerization is electron spin resonance (ESR) spectroscopy. ESR has been applied for many years to the study of bulk polymerization reactions,[15−21] but recently it has been shown that ESR can be used to study the propagating radicals in batch and semicontinuous emulsion polymerization.[22−26] More recently, Lau and Westmoreland[27] have developed a closed-loop flow system which has been used to monitor the concentration of propagating free radicals by ESR in semicontinuous emulsion polymerization as the reaction is proceeding. We have further developed the flow system methodology to be applicable to batch emulsion polymerization.[28] These further developments included the use of time sweep rather than field sweep techniques to collect ESR data points more rapidly and gravity flow of the polymerizing latex into a collection reservoir to avoid polymer gel formation in the recycling flow system. Using these methods, we can now monitor the rapidly changing propagating free-radical concentration essentially in real time during batch emulsion polymerization of MMA, which allows measurement of critical kinetic parameters. In addition, we could make inferences about the nature of the propagating radical distribution inside the latex particles.

Experimental Details

Material. Sodium sulfoxylate formaldehyde (SSF, 99%) and MMA containing 10 ppm methoxyphenol (MEHQ) were obtained from Rohm and Haas Co. Sodium dodecyl biphenyloxide disulfonate (Dowfax 2A1) was obtained from Dow Chemical Co. as a 45% aqueous solution. Sodium persulfate (NaPS) was obtained from Aldrich Chemical Co. In-house deionized water was further purified with two ion exchange columns. Nitrogen (≥99.8%) was obtained from Air Products, Industrial Grade UN 1066.

Emulsion Polymerization of MMA with Various Particle Sizes. The equipment setup of batch emulsion polymerization in conjunction with ESR monitoring and latex analyses have been described previously.[27,28] The following is a general procedure used for these polymerizations in which particle size was varied; detailed synthesis recipes for each particle size are given in Table 1.

The polymerizations were carried out under nitrogen atmosphere. The ingredients in the "kettle charge" are stirred and heated to 50 °C with a circulating water bath. Then the

† Present address: Industrial Technology Research Institute, Hsinchu, Taiwan.

⊗ Abstract published in *Advance ACS Abstracts,* June 15, 1996.

S0024-9297(95)01652-4 CCC: $12.00

Table 1. Ingredients for Batch Emulsion Polymerization of MMA for Various Particle Sizes[a]

	particle size (nm)				
	80	110	170	230	400
Kettle Charge					
deionized water	2234	2376	2005	2334	2105
seed latex	0	0	443.8	69.4	380
part. size, nm			92	107	256
solids, %			16.4	40	43.9
Dowfax 2A1 (45%)	51.82	0	0	0	0
Monomer Emulsion					
deionized water	148	148	135	148	135
Dowfax 2A1 (45%)	6.05	12.09	5.56	6.05	5.56
MMA	544	544	500	544	500
rinse water	150	150	150	150	150
Initiators					
SSF	0.408	0.408	0.375	0.408	0.375
deionized water	28	28	28	28	28
NaPS	0.408	0.408	0.375	0.408	0.375
deionized water	28	28	28	28	28

[a] All weights in grams.

seed latex is charged to the kettle where applicable. The emulsified monomer is then poured into the reactor at once, and the system reaches a temperature of ~45 °C. About 2 min later, SSF and NaPS solutions are added sequentially. ESR recording of the reaction (time zero) starts at the moment the NaPS solution is added. Samples for intermittent conversion and particle size analysis are taken from the kettle and are preserved by two drops of MEHQ solution (6.25% in 2:1 water/methanol). As the polymerization reaction begins, the contents of the kettle are allowed to flow continuously by gravity through the ESR cell and the ESR signal is collected at the set magnetic field every 2.6 s.

Monomer Preswelling Experiment. Two 230-nm particle size polymerizations were carried out on the same day: one reaction was carried out with the usual 2-min delay between addition of monomer emulsion and addition of initiator, while the second reaction was carried out with a 2-h delay between addition of monomer emulsion and initiator; the reaction mixture was maintained at 50 °C during the 2-h period.

Seeded Small Particle Size Polymerization. In the seeded run, 5% monomer and 80% total surfactant were used to generate 36-nm seed particles. The rest of the monomer and surfactant was then added. The final particle size was 96 nm. Since the 80- and 110-nm systems show qualitatively similar behavior in the shape of the radical signal data, we expect that the 96-nm seeded and 110-nm unseeded runs are comparable for our purposes. The total surfactant level, initiators, and temperature were kept the same for the seeded and unseeded runs.

Analysis of Latex Samples. Monomer conversion was analyzed by either solid content (gravimetric method) or residual monomer analysis by GC in the case of the very high conversion region in some runs. Latex particle size was measured by light scattering on a Brookhaven BI-90 instrument.

ESR Studies. ESR spectra were collected with a Bruker ESP-300 ESR spectrometer at X-band using a custom-built flat cell with dimensions 0.3 mm thick by 13 mm wide. The temperature in the sample cavity was controlled by a Bruker ER 4111 VT temperature controller. Typical conditions for acquisition of ESR spectral data were cell temperature, 55 °C; microwave power, 2 mW; and modulation amplitude, 5.05 G. For a time-averaged field sweep, 25 scans were collected. For a field fixed-time sweep experiment, data points were collected every 2.6 s.

The concentration of free radicals in the samples analyzed was calculated by comparison with solutions of the stable nitroxide radical TEMPOL (4-hydroxy-2,2,6,6-tetramethylpiperidine-*N*-oxyl).

The general procedure for the time sweep experiments is to sit on one of the two strongest peaks of the PMMA propagating radical ESR signal (see Figure 1 for a typical spectrum) and monitor the change in peak height during the polymerization reaction. At the end of the run, a field sweep ESR spectrum is collected corresponding to the peak height at that moment. The area of this spectrum is integrated and compared to the TEMPOL calibration curve. The radical concentration for this peak height is then used as a reference point for calculating the radical concentration based on total emulsion volume for the entire run. After normalizing by the percent of solids in the emulsion, the radical concentration based on the organic phase used in this report is obtained.

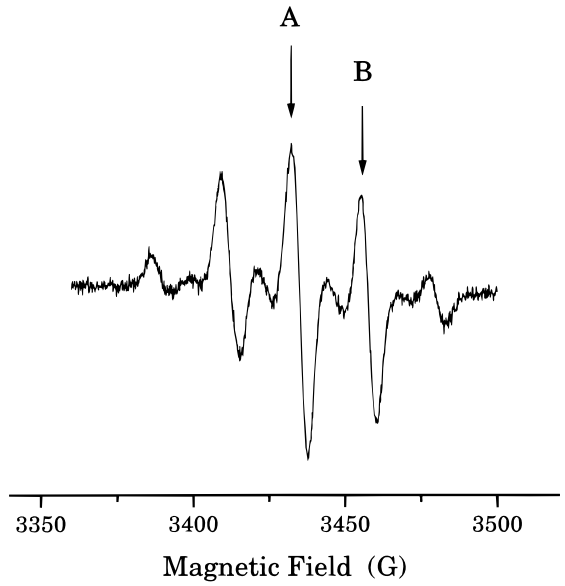

Figure 1. ESR spectrum for PMMA propagating free radical observed during 230-nm polymerization shown in Figure 4. A and B indicate field positions used in time sweep experiments.

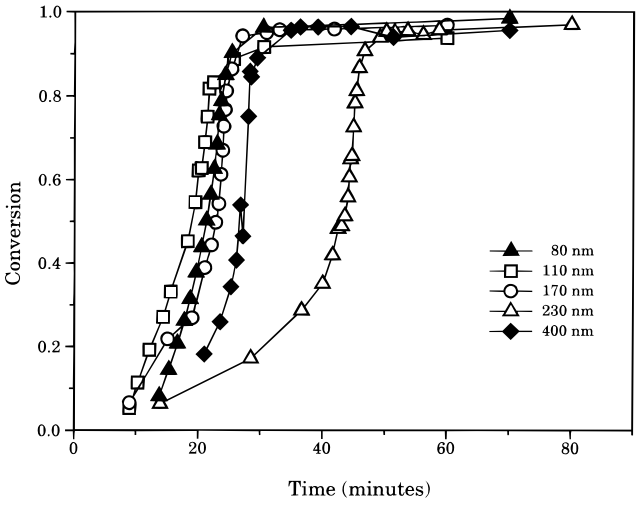

Figure 2. Conversion vs time for various particle size polymerizations.

Results

Careful control of experimental conditions is crucial for getting consistent results for emulsion polymerizations. In this study we usually ran the reaction at least three times for each different emulsion polymerization process. In general, the reproducibility was good.

Conversion and Temperature Profiles. Representative monomer conversion profiles for MMA batch emulsion polymerization at various particle sizes are shown in Figure 2. Generally, the conversion at the end of the polymerization is above 95%. The corresponding temperature profiles of these processes are similar, all initiated at 45 °C, and reaching a peak temperature of ~58−60 °C at ~93% conversion and then slowly cooling to room temperature at the end of the reaction.

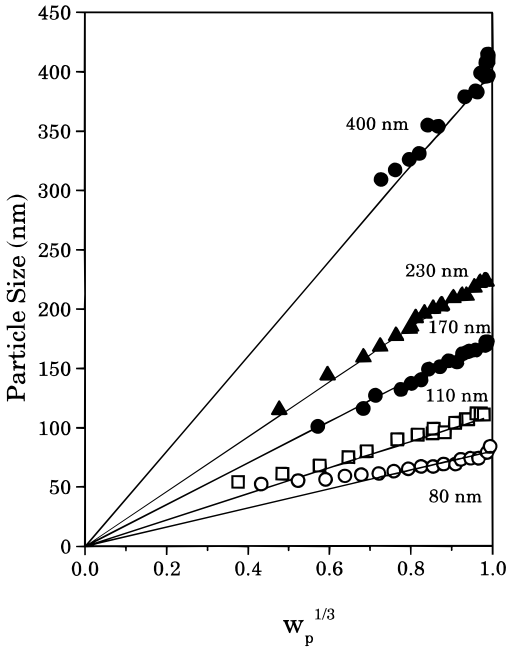

Figure 3. Particle size vs $w_p^{1/3}$ for various particle size polymerizations.

The data show that particle size affects several aspects of the polymerization kinetics. First, the polymerization rate at low conversion is affected by both the particle size and the amount of seed polymer present in the system. In our experiments, the rate at low conversion is generally decreased by increasing particle size and increased by increasing the amount of polymer seed. For example, the 80- and 110-nm sizes have higher rates at low conversion (<30%) than the larger particle sizes (Figure 2). On the other hand, the presence of polymer seed will increase the rate at low conversion. This polymer seed effect can be rationalized in terms of the weight fraction of polymer starting closer to the Trommsdorf region. In Figure 2 the data of 170−400 nm systems do not follow a consistent pattern because the effects of particle size and various amount of polymer seed used in each experiment counteract each other.

The rate of polymerization in the Trommsdorf region is also influenced by the particle size. Our data show a slight increase in rate when particle size is increased. This is most noticeable in the 80-nm experiment where the temperature rise and monomer conversion do not show the near-vertical rise like the larger particle size cases.

Particle Size. In this work, particle size variation is achieved by varying the amount and/or size of the seed latex and/or surfactant level (see Table 1 under Experimental Details). The particle size distribution of final latex particles for each particle size polymerization in this study was unimodal.

Particle size at various monomer conversions was obtained from inhibited samples withdrawn from the reactor. The measurement was done under very dilute conditions and the particle size values obtained are closer to a polymer-only particle rather than a monomer-swollen particle. To illustrate the relation between particle size and monomer conversion more clearly, the particle size of each run is plotted against the cube root of the polymer weight fraction in the monomer−polymer mixture, w_p (Figure 3). In the case of nonseeded runs, w_p equals conversion. In the case of seeded runs, w_p includes the seed polymer portion. If no new particles

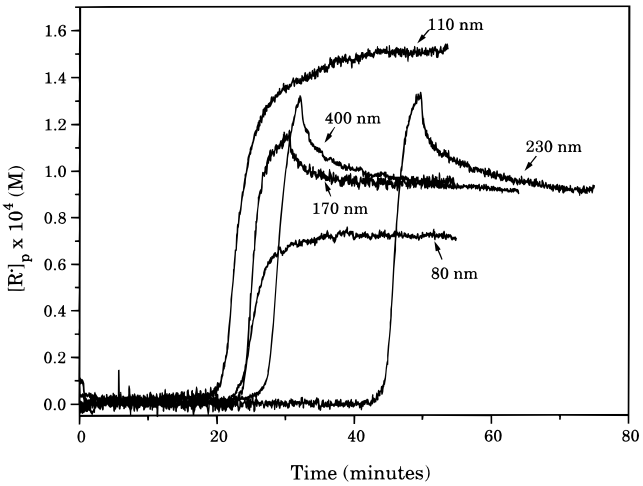

Figure 4. $[R^\bullet]_p$ vs time for various particle size polymerizations.

are created, there should be a linear relation between particle size and $w_p^{1/3}$ according to eq 1 and indicated by the straight lines in Figure 3.

$$\frac{D_t}{D_{\text{final}}} = \left[\frac{W_t}{W_{\text{final}}}\right]^{1/3} = (w_p)^{1/3} \tag{1}$$

Examining the results from 80 to 400 nm (Figure 3), we find that the 170-, 230-, and 400-nm series all show good agreement between the actual particle diameter and the predicted linear relation. This indicates that the particle numbers are constant throughout the polymerization reactions. The 80- and 110-nm runs show a deviation above the predicted linear relation at lower conversions but a good match at higher conversions. This behavior suggests that the particle size at low conversion is larger and the particle number is lower than that predicted at the beginning of the reaction. More particles are nucleated as the reaction proceeds and eventually reach a stable number. From the data in Figure 3, this stabilization point for the 80-nm runs is at ∼42% conversion (or $w_p^{1/3} \sim 0.75$) and for the 110-nm runs is at 22% conversion (or $w_p^{1/3} \sim 0.6$).

Another possible explanation for the deviation observed in the 80- and 110-nm runs is that the particles at low conversions are unstable due to their small size (<50 nm) and the presence of a large amount of unreacted monomer. Particles becoming increasingly swollen by monomer or even coalescing might have occurred before the samples were analyzed.

Radical Concentration. The ESR signal of the propagating free radicals in the batch emulsion polymerization of MMA was continually monitored during the synthesis. Figure 4 shows representative plots of the PMMA propagating radical concentration, based on the total volume of monomer and polymer, $[R^\bullet]_p$, as a function of the reaction time for various particle sizes. Figure 5 shows the same radical concentration plotted against overall polymer fraction w_p. The important feature of the data in Figure 4 is the shape of the curves rather than the relative position of the curves on the time scale.

The ESR results for the 80- and 110-nm particle size polymerizations are qualitatively similar. The propagating radical concentration starts to increase noticeably after ∼20 min (∼40% conversion), but the most rapid increase occurs in the range of 80−90% conversion. Even after the reaction is almost complete, $[R^\bullet]_p$ for both the 80- and 110-nm particle size polymerizations con-

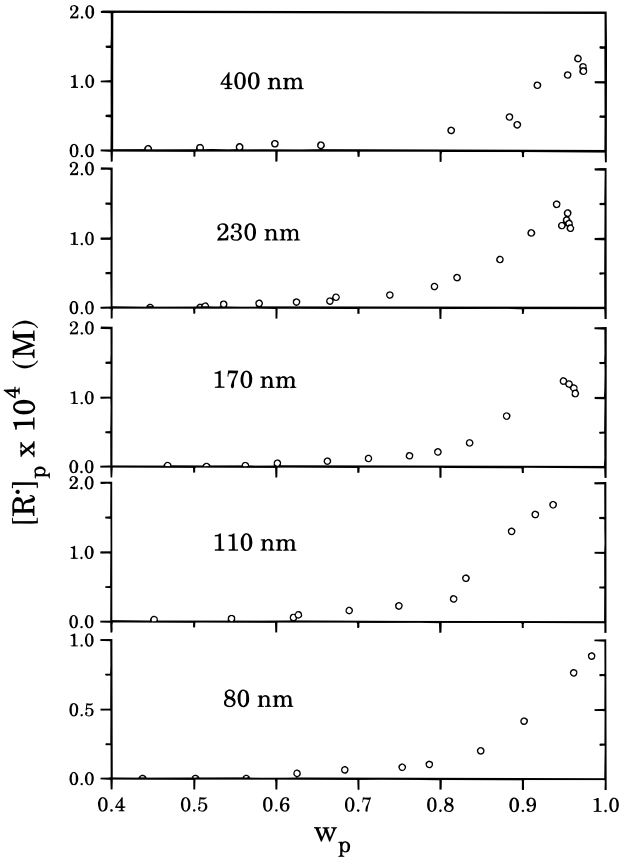

Figure 5. $[R^\bullet]_p$ vs w_p for various particle size polymerizations.

tinues to maintain its maximum value within the ~1 h observation time.

The behavior of the propagating radical concentration for larger particle sizes (170, 230, and 400 nm) is significantly different from that of the 80- and 110-nm cases (Figures 4 and 5). Although the maximum $[R^\bullet]_p$ is about the same as that of the 110-nm case, a rapid decrease in the propagating radical concentration is observed shortly after the maximum $[R^\bullet]_p$ value is reached. As shown in Figure 5, $[R^\bullet]_p$ maximizes at a w_p of 0.93−0.96. The relative amount of rapid radical concentration decrease is ~20% from its maximum value for 170 nm, ~30% for 230 nm, and ~35% for 400 nm. As the particle size increases from 170 to 230 nm, the rate of decrease in the propagating radical signal is also faster. For all three particle sizes, a second region of more gradual $[R^\bullet]_p$ decrease is also observed (Figure 4).

Calculated Average Number of Radicals per Particle, $\bar{n}$. The average number of radicals per particle at any conversion can be calculated directly from the radical concentration based on total emulsion volume, $[R^\bullet]$, the conversion x, and the particle size value D_t, all obtained experimentally.

$$\bar{n} = \frac{[R^\bullet]V_E}{N_p} = \frac{[R^\bullet]V_E N_A \rho_p \pi (1/6)(D_t)^3}{(xW_{final} + W_{seed})} \qquad (2)$$

The maximum $\bar{n}$ value observed for each particle size is listed in Table 2. Plots of $\bar{n}$ as a function of w_p for various particle size runs are shown in Figure 6. In the 80-nm case, $\bar{n}$ is less than 1 up to 60% w_p and reaches a maximum value of 14 at the end of the run. For the 110-nm polymerization, $\bar{n}$ is less than 1 up to ~40−60% w_p and maximizes at 75 at the end of the run. At particle sizes of 170 nm and above, $\bar{n}$ increases dramatically at ~40% w_p and then declines after having reached a maximum at ~90% w_p. In 170-nm runs, the maximum $\bar{n}$ reaches a value of ~250. The maximum $\bar{n}$ value reaches almost 600 for the 230-nm runs and 3000 for the 400-nm runs. Although $\bar{n}$ values increase rapidly as particle size increases, the average volume each radical occupies ($\bar{V}_R$) is about the same for all the particle size polymerizations except 80 nm (see Table 2). The minimum detectable concentration of PMMA propagating radicals in our emulsion polymerization system by ESR is ~3 × 10^{-7} mol/L expressed on emulsion volume. This limit determines a lowest detectable $\bar{n}$ for each particle size (see Table 2). The accuracy of the measured value for $\bar{n}$ increases as the radical concentration increases.

Table 2. Maximum $\bar{n}$, Minimum Detectable $\bar{n}$, and Average Volume per Radical for Various Particle Size Polymerizations

particle size, nm	$\bar{n}_{max}$[a]	$\bar{V}_{R^\bullet}$,[a,b] nm^3 (×10^{-3})	min detectable $\bar{n}$
80	14 (±3)	19 (±5)	0.4
110	73 (±9)	10 (±3)	1
170	240 (±32)	11 (±1)	2
230	590 (±74)	11 (±1)	6
400	3000 (±210)	11 (±1)	50

[a] The (±) values for $\bar{n}$ and $\bar{V}_{R^\bullet}$ are one standard deviation calculated from the replicate runs. [b] $\bar{V}_{R^\bullet}$ is the average volume that each radical occupies.

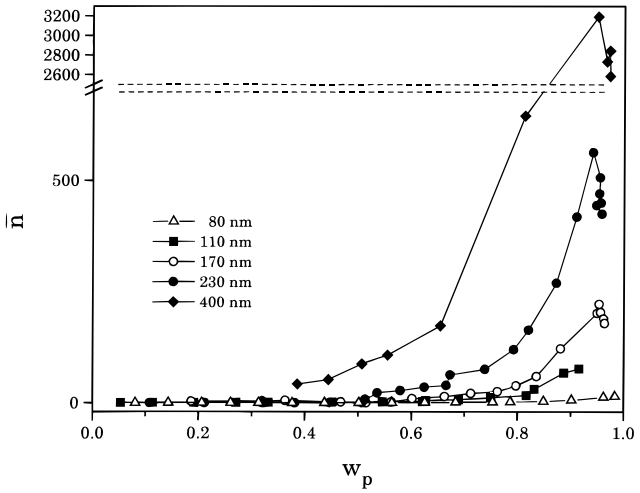

Figure 6. $\bar{n}$ as a function of w_p for various particle size polymerizations.

Extended Observation of Radical Termination. In order to fully characterize the nature of radical termination processes observed in large particle size polymerizations and to investigate the nature of unterminated radicals in the small particle sizes at longer times during the polymerization, we extended the observation time from ~1 h to 3 h or more in an experiment we call a "long-hold" run. The long-hold experiments were carried out as usual with gravity flow as described above. Shortly after reaching the peak radical concentration, the flow of latex was stopped. The latex contained in the ESR cell was maintained at either 55, 65, or 75 °C for prolonged observation of radical termination. At this later stage of the batch reaction, the monomer droplets have all disappeared, the rapid temperature change has long passed, and the polymerization is concluding in the polymer particles; thus we assume that the reaction will proceed in the ESR flow cell in the same way that it would have been proceeding in the reactor at the corresponding temperatures.

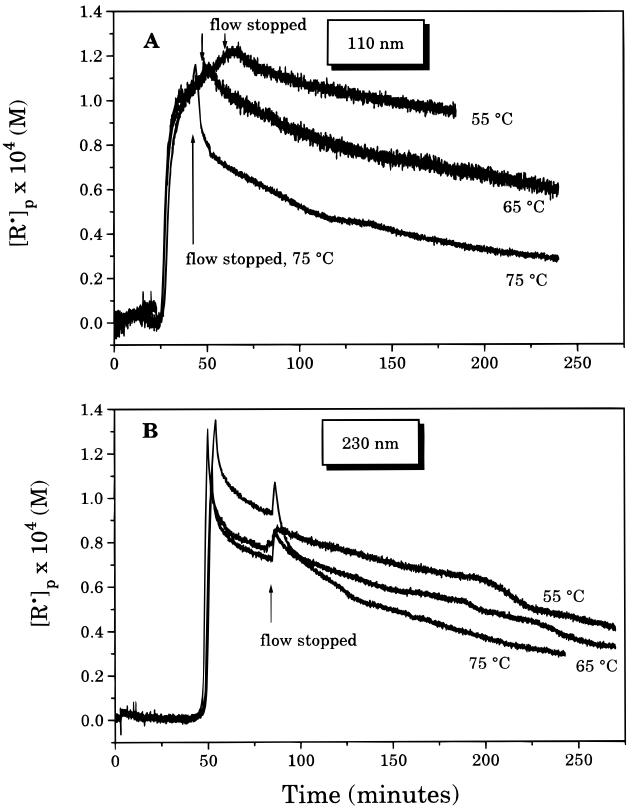

Figure 7. $[R^\bullet]_p$ vs time for (A) 110- and (B) 230-nm particle size polymerizations held at 55, 65, and 75 °C during radical signal decrease.

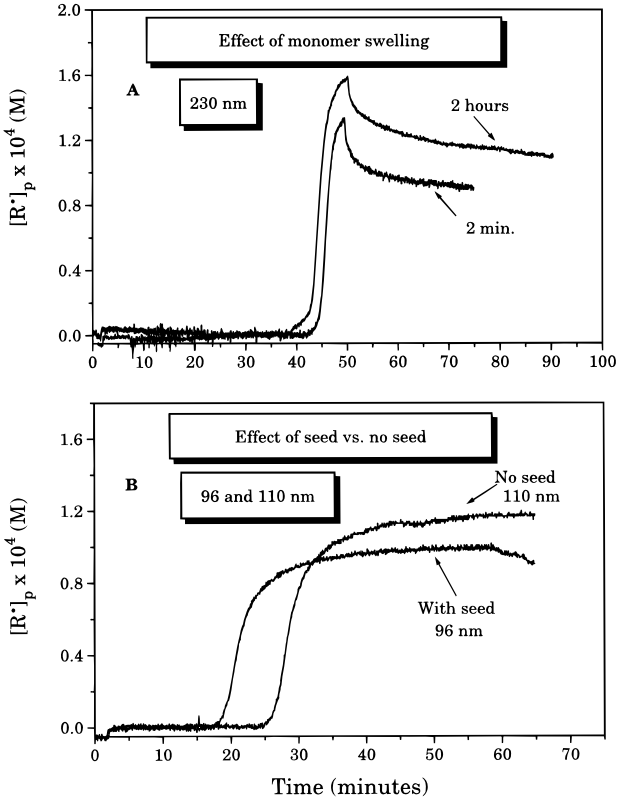

Figure 8. Control experiments for (A) the effect of monomer swelling and (B) the effect of seed.

Figure 7 shows representative runs for 110- and 230-nm latexes at various holding temperatures. For the 110-nm particle size experiment, the flow was stopped in the range of 42−60 min for the three temperatures studied (see Figure 7A). When the flow is stopped, a small disturbance in the radical signal is observed. Various experimental factors are probably responsible for the observed change in the signal (peak height), including small changes in temperature which change the spectrometer tuning; the temperature is not fully equilibrated in the flow cell during rapid flow but reaches the exact cell temperature when flow stops. The important feature of the 110-nm long-hold experiment at 55 °C is that a slow steady decline in the radical signal is observed after ∼75 min from the start of the experiment. In our early experiments of less than 60 min in total observation time, this behavior was missed.

In the case of the 230-nm experiment, the flow was stopped at 85 min for the three temperatures studied (see Figure 7B). When the flow is stopped, a noticeable disturbance in the radical signal is observed; we expect that similar experimental factors are involved although the size of the disturbance is somewhat larger than for the small particle size system. Aside from the disturbance, we observe a continuation of the radical termination which has already begun at the early part of the experiment.

For both particle sizes the rate of radical termination increases as the ESR cell temperature increases. Also, the radical termination rate for both particle sizes at longer times at each temperature is about the same (Figure 7).

Effect of Monomer Preswelling at 230 nm. The very different radical termination behavior observed in our 110- and 230-nm particle size experiments might conceivably be due to inhomogeneity in the polymer particles resulting from incomplete equilibration of monomer swelling into the seed polymer. To investigate this possibility, we estimated (eq 3) the amount of time

$$D_{\text{diff}} = r^2/6t \tag{3}$$

needed for MMA monomer to diffuse into the center of the particle using the known diffusion coefficient for MMA in PMMA.

Since the diffusion coefficient of MMA is a function of w_p, the MMA diffusion rate is expected to accelerate as more and more monomer diffuses into the particle. In the worst case of MMA diffusing into a "dry" PMMA particle at 45 °C ($D_{\text{diff}} = 2 \times 10^{-14}$ cm^2/s, obtained from ref 29), the time to travel 50 nm (radius of the polymer seed) is only ∼200 s, much shorter than the time of observing any significant radical signal. Therefore, we do not think that monomer diffusion into the seed particle is the cause for the inhomogeneity we propose. The experiment in which we let MMA swell into the seed for 2 h prior to initiator addition strongly supports that conclusion.

Figure 8A shows a comparison of the radical concentration data for these two 230-nm particle size runs. Some variability in the onset time for $[R^\bullet]_p$ increase and the maximum value of $[R^\bullet]_p$ was observed; however, the general qualitative behavior of the radical concentration vs time profile is the same. In particular, the qualitative form of the decrease in radical concentration right after the peak radical signal is very similar for the two runs; we generally observe some small variations among replicate runs and so cannot be certain that the apparent small difference in the decreasing signal portion of the radical concentration plots is outside experimental variation. Thus we conclude that the prolonged monomer swelling did not change the radical termination behavior relative to the differences observed between 110- and 230-nm systems.

Table 3. GPC Molecular Weights of PMMA for Various Particle Sizes[a]

	molecular weight of final samples		
particle size, nm	$M_w \times 10^{-6}$	$M_n \times 10^{-6}$	M_w/M_n
80	7.0 (±0.8)	2.3 (±0.2)	3.0
110	5.6 (±0.8)	1.4 (±0.2)	4.1
170	3.2 (±0.1)	0.74 (±0.05)	4.3
230	3.0 (±0.2)	0.6 (±0.1)	5.2
400	3.0 (±0.3)	0.67 (±0.06)	4.8

[a] Numbers in parentheses are standard deviations from replicate runs.

Seeded Small Particle Size Polymerization. Another question is the possibility that use of a seed polymer might conceivably affect the radical termination reaction. Therefore, we carried out an experiment for a small particle size latex in which we polymerized with and without a seed polymer. Figure 8B shows the radical concentration vs time profiles for the runs with and without seed. The results of the two reactions do not indicate any major differences in the shape of the curves; although the seeded reaction shows a slightly faster "takeoff" than the nonseeded run. Comparing the results obtained with or without the seed (Figure 8B), we see that small particle size reactions do not have the immediate radical signal decrease that is seen in the large particle size reactions. Thus the seed does not account for the differences in behavior between the small and large particle size systems. Some decrease in the radical signal is seen for the seeded run at very late time. We know from the long-hold experiments that radical signal decrease is observed in the small particle size systems when the observation time is extended. So since the seeded run has an earlier exotherm, it reaches a point where termination begins to be observed earlier than the unseeded run, which does not show any decrease in signal in the observation time of this particular experiment.

Molecular Weight Analysis. An initial analysis of the final molecular weights of some of the various particle size latexes was carried out to see if any differences could be observed in this important polymer parameter. Table 3 summarizes the M_w and M_n values for the various particle size latexes. The data show that particle size has a very significant effect on both the polymer molecular weight and molecular weight distribution. M_w almost doubles when the particle size is reduced from 230 to 110 nm. Furthermore, the molecular weight distribution is narrower in the polymers made with smaller particle size. Molecular weight distribution as a function of monomer conversion has also been determined by quenching intermittent conversion samples. The detailed molecular weight results and a subsequent analysis of molecular weight distribution in conjunction with the radical termination mechanisms will be discussed elsewhere.[30]

Effect of Surfactant. The possibility of an effect of the surfactant used in the polymerization has been considered. In the results shown above for variation of molecular weight with particle size, the highest molecular weights were achieved for the smallest particle size system, which uses the most surfactant. This result implies that chain transfer to surfactant is not a significant factor in this system.

Discussion

Rate of Monomer Conversion. Our results have demonstrated that the rate of MMA polymerization in a batch emulsion process is significantly influenced by the size of the latex. The rate of conversion is slower in larger particles at low conversions because there is a higher rate of radical termination in the larger particles. This can be qualitatively understood by recalling that the large and small particle size experiments were run with the same total volume of monomer, the same volume of water, and the same amount of redox initiator. The only difference was in the size and number of the particles. As particle size is doubled from 100 to 200 nm, the number of particles decreases by a factor of 8 for a constant volume of monomer. We assume the same initiator radical flux and also the same radical capture efficiency for the two systems, since there is essentially 100% initiator efficiency for MMA polymerization,[13,31,32] which would imply that ~8 times the number of radicals enter per unit time into a large particle compared to a small particle. During this initial stage of the polymerization, the viscosity of the particle interior is low and the propagating radicals will be able to diffuse rapidly and terminate. In the large particle, the radicals that remain in the particle will terminate more rapidly. However, in the small particle system, there are 8 times fewer radicals entering each particle per unit time and so the probability of radical termination is lower.

Of course, propagation is also occurring during this initial stage of the reaction. However, the propagation rate is slower than the termination rate in the large size particles, and therefore, the overall rate of monomer conversion is very low. In contrast, smaller particles experience a longer time interval between each radical entering event, and the resulting longer lifetime for each propagating radical allows the polymerization to continue longer relative to the large particle case.

The ESR data were not able to provide direct evidence for the above hypothesis. As shown by eq 4, the overall

$$R_p = -\frac{d[M]}{dt} = k_p[M]_p[R^\bullet]_p \qquad (4)$$

rate of polymerization, R_p, which is equal to the monomer conversion rate, is a function of the propagation rate coefficient, the monomer concentration in the particles, and the radical concentration in the particles. Since $[M]_p$ can be measured experimentally and k_p is expected to be independent of particle size, especially at low conversion, our ESR technique should allow us to determine whether the low monomer conversion rate seen in the large particle size polymerizations is due to a low $[R^\bullet]_p$. Unfortunately, during the early period of the reaction the ESR signal for the propagating radicals is below our detection limit, and so we cannot verify whether the initial $[R^\bullet]_p$ does vary with particle size. However, we can find support for our hypothesis from molecular weight data.[30]

Equation 4 assumes that all propagating radicals are counted, that all polymerization occurs in the latex particles, and that the propagating radicals are homogeneously distributed in the latex particles. In systems where these conditions are not fully met, then the equation must be modified; for example, use of the equation to calculate k_p in those circumstances would yield an "effective" k_p rather than a classical literature value. In using ESR to determine the value of $[R^\bullet]_p$, we assume that the 9-line spectrum we observe represents all of the radicals present and that the radicals observed are all propagating radicals. Recently Tian et al.[33] speculated in using ESR to study bulk polymerization of MMA with cross-linker that the 9-line ESR spectrum is due to "trapped" radicals that are not

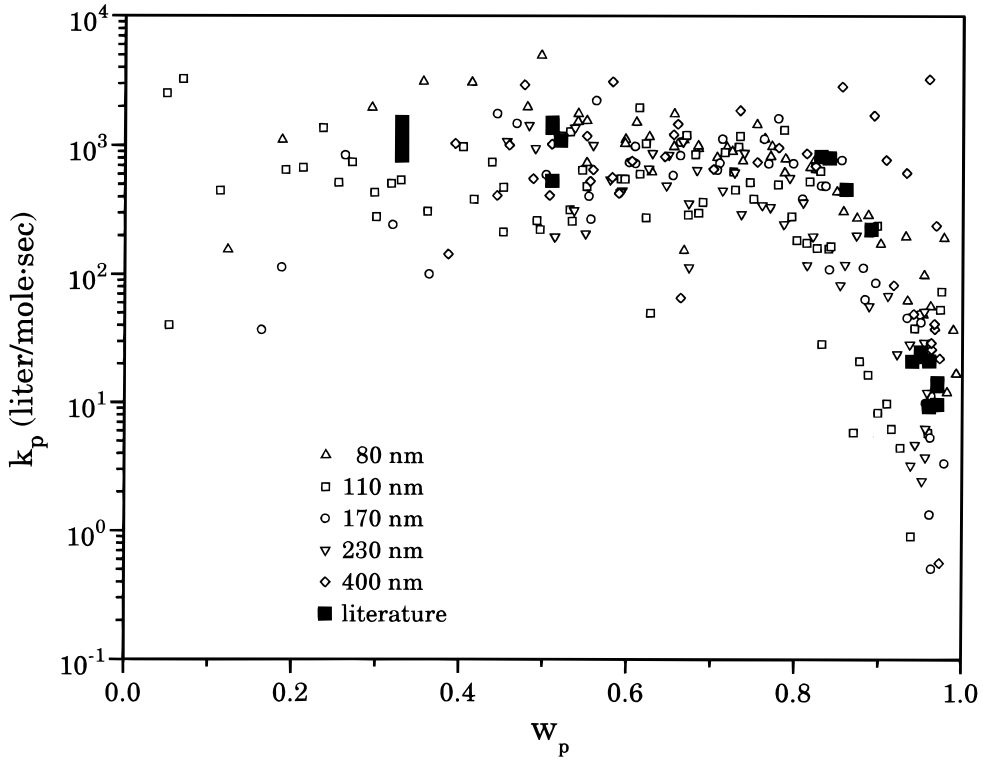

Figure 9. Comparison of k_p as a function of w_p for our various particle size polymerizations and literature values.[23]

actively propagating, while a 13-line ESR spectrum represented the actual propagating radicals. However, subsequent work by two independent groups, Shen et al.[19] and Tonge et al.[34], has demonstrated that the only difference between radicals represented by the two ESR spectra is their relative mobility. The 13-line spectrum is due to mobile, oligomeric propagating radicals and the 9-line spectrum is due to relatively immobile, polymeric propagating radicals. In our studies we have always observed only the 9-line spectrum, due to the fact that essentially all the propagating radicals are polymeric in nature when we reach a w_p where we can observe the ESR signal.

Another effect for which we observed particle size variation was behavior in the Trommsdorff region. The rate of monomer conversion, and of temperature increase, is less rapid in the 80-nm particle size polymerizations than in the larger particle size polymerizations. A first-order explanation can be made by reference to eq 4. In the Trommsdorff region, the 80-nm particle size polymerization has slower monomer conversion rate than in other larger size polymerizations. Also, we found that the maximum $[R^\bullet]_p$ in the 80-nm runs is only about half that observed for larger particle sizes. Since the rate of monomer conversion is dependent on the monomer concentration and the radical concentration, the slower rate acceleration in the Trommsdorf region observed in the 80-nm particle size runs may be partially due to the lower radical concentration. So far we have not found any simple explanation for the lower radical concentration observed for the 80-nm particle case.

We can calculate the effective propagation rate coefficient k_p at intermediate and high conversion in our polymerizations using eq 4. Since we are able to measure $[M]_p$, $[R^\bullet]_p$, and $d[M]/dt$ experimentally, we can calculate k_p as a function of w_p for various particle sizes.[35] When all the values of k_p from replicate runs of various particle size polymerizations are plotted against w_p, one curve is obtained (Figure 9). The results indicate that k_p as a function of w_p is, within our experimental error, independent of particle size in this system. Comparing our values to the literature values of k_p for MMA emulsion polymerization,[23] we find good agreement.

Propagating Radical Termination and Inhomogeneity in Radical Distribution. We observed a decrease in the ESR propagating radical signal occuring at very high conversions ($x > 0.9$) which is particle size dependent. This radical signal decrease occurs earlier, faster, and to a larger extent when the particle size is increased (Figure 4). We surmised that the decrease in radical signal is a result of termination and systematically explored some potential causes for the decrease. We first ruled out the possibility of oxygen leaking into the system. Faster termination due to temperature rise at the exotherm was ruled out by noting that the polymerization temperature profiles for various particle sizes are essentially identical. We have also considered any surface-related termination events such as radical desorption and then termination in the aqueous phase. Although we have no detailed information about these aqueous phase events, we do not think it is very likely to be the cause for the radical signal decrease because the propagating radicals are practically immobile above 90% conversion. Besides, the highest amount of signal decrease is observed in the largest particle size samples, which have the lowest total surface area (see Table 4 below).

Our explanation of the differences in various particle size polymerizations in radical termination is that there is an inhomogeneous distribution of propagating radicals in the large particles and negligible inhomogeneity in the small particles. Inhomogeneous radical distribution has been invoked previously in certain situations for emulsion polymerization.[11,13,14,24] Radical termination rates would be accelerated in the larger particle size polymerizations due to higher local $[R^\bullet]_p$ caused by the higher inhomogeneity of the propagating radical distribution. Furthermore, we hypothesize that a larger

Table 4. PMMA Radical Signal Decrease in Various Particle Size Latexes[a]

particle size, nm	A_s, nm^2 ($\times 10^{-22}$)	$[R^\bullet]_{p,max}$, mol/L ($\times 10^4$)	w_p[d]	$\Delta[R^\bullet]_p/[R^\bullet]_{p,max}$, %	$\Delta[R^\bullet]_p/A_s$, mol/L·nm^2 ($\times 10^{-27}$)	$\bar{V}_{R^\bullet}$, nm^3 ($\times 10^{-3}$)	$\bar{V}_{R^\bullet,inhomo}$, nm^3 ($\times 10^{-3}$)
80	2.74	0.6	n/a[b]	n/a	n/a	19	19
110	2.32	1.7	0.98	10	0.7	9.5	9.3
170	1.61	1.4	0.95	19	1.7	11	9.1
230	1.09	1.5	0.94	29	4.0	11	7.8
400	0.68	1.6	0.93	26	6.1	11	5.5

[a] A_s is total surface area of all the particles in the reactor. $\Delta[R^\bullet]_p$ is the relative decrease in radical concentration based on the maximum radical concentration. w_p[d] is the polymer fraction in the particles when $[R^\bullet]_p$ starts to decay. $\Delta[R^\bullet]_p/A_s$ is the relative radical concentration decrease per surface area. $\bar{V}_{R^\bullet}$ is the average volume each radical occupies, and $\bar{V}_{R^\bullet,inhomo}$ is the average volume each radical occupies assuming all the radicals are located in the outer 40-nm layer in the particle. [b] n/a, not available.

fraction of the radicals is located near the surface, which makes them more susceptible to being terminated by radicals entering from the aqueous phase.

At very high conversion, the majority of the radicals are long and immobile and they can terminate in several different ways. One is recombination with a short oligomeric radical entering the particle from the aqueous phase. Such termination will most likely occur for those radicals located near the surface. This type of termination has been referred to as "short−long termination" in the literature and is more generally a subset of so-called chain-length-dependent termination.[4,5] If these entering oligomeric radicals are not consumed by encountering an immobile radical, they will quickly become immobile themselves due to propagation into longer chains. Another way to terminate the immobile PMMA radicals is by a "residual termination" process, a term used to describe termination of two immobile radicals that move close enough together to terminate through propagating with residual monomer.[36]

Both short−long and residual termination depend on radical concentration. The higher the radical concentration, $[R^\bullet]_p$, the faster the termination rate. As shown in Table 4, the overall radical concentration expressed on particle volume basis is essentially the same for 110−400-nm particle sizes, but the relative amount of radical signal decease based on the maximum radical concentration, $\Delta[R^\bullet]_p/[R^\bullet]_{p,max}$, and the amount of the radical signal decrease per particle surface area, $\Delta[R^\bullet]_p/A_s$, increase as the particle size increases. As the data in Table 4 show, the largest radical signal decrease occurs in the largest particle size, which has the lowest total surface area. Since the radical signals we observed by ESR in these studies are for relatively immobile polymeric radicals, one could argue that there might be a difference in the concentration of the mobile oligomeric radicals in various particle size polymerizations (although the steady state concentration of these mobile radicals must be low, since we do not detect any contribution from the 13-line ESR spectrum which they would show). From the reaction conditions, we expect that the aqueous phase oligomeric radical concentration is a function of initiator decomposition rate. At an equivalent time during the reaction, the oligomeric radical concentration is assumed to be the same for different particle size polymerizations. Our results show that at the time when the radical signal in the large particle size polymerizations starts to decrease, there is no detectable signal loss at all in the small particle size runs. Therefore we consider it unlikely that the radical signal decreases due to differences in oligomeric radical concentration.

The dramatic difference in the radical termination behavior in various particle size polymerizations can be explained by an inhomogeneous distribution of propagating radicals throughout the particles. Theoretical modeling by Mills et al.[9] has predicted that in some circumstances there is a radical concentration gradient along the particle radius, with the radicals being more concentrated near the surface than in the center. As the particle size increases, the radical inhomogeneity increases with particle radius and with w_p. Their calculation shows a significantly higher radical concentration in roughly the outer 30 nm of a 500-nm particle for the case of PMMA at very high conversion. This inhomogeneous radical distribution will change the volume that each radical occupies, $V_{R^\bullet}$. As shown in Table 4, if we assume all the radicals are distributed uniformly in the particle, then the average volume each radical occupies, $\bar{V}_{R^\bullet}$, is about the same for 110−400 nm particles. However if the radicals are mostly located in a thick crust at the surface of the particle, the average volume each radical occupies would be significantly smaller and it would be particle size dependent. An illustrative example assuming that all radicals are residing in a 40-nm-thick crust is shown in Table 4. As the $\bar{V}_{R^\bullet,inhomo}$ values illustrate, the radicals become increasingly closer to each other as particle size increases.

If there is an effect of limitation of kinetic processes by diffusion in this system, then radical inhomogeneity increases as the particle size increases, because the diffusion limitation is more pronounced in larger particles. In the region of the particle where $[R^\bullet]_p$ is higher, the radicals are relatively closer to each other, which makes termination by either residual or short−long mechanisms more favorable. Therefore, as the polymer fraction w_p increases, $[R^\bullet]_p$ builds up near the surface and eventually reaches a point where rapid termination outweighs the radical buildup, so that the overall $[R^\bullet]_p$ starts to decrease. When particle size is 110 nm or smaller, the propagating radical inhomogeneity is negligible. Only the slower residual termination process is observed at $w_p \sim 0.98$; whereas in the larger particles a fast termination, possibly dominated by the short−long mechanism, is observed as early as $w_p = 0.93$ for the 400-nm case (Table 4). Our experimental results provide direct evidence of faster radical termination in larger particles, which is consistent with the theoretical prediction of Mills et al.[9]

As described in the Results section, we carried out some long-hold experiments to observe the radical signal decrease behavior in two different particle size latexes. The radical decrease data from these experiments can be fitted mathematically in order to obtain information about the radical termination mechanism and termination kinetic parameters.[37] The results of this analysis indicate that at extended reaction times residual termination dominates in both small and large particle size systems. Estimation of the termination rate coefficients at 55, 65, and 75 °C yields an activation energy for the bimolecular termination process at extended reaction times of ~25 kcal/mol.[37] A more complex behavior is observed in the sharp drop which occurs just after

maximum radical concentration is reached for the large particle size systems; in this region both short−long and residual termination mechanisms are probably involved.

Conclusions

In this work a unique setup was used to continuously monitor propagating radical signals in batch emulsion polymerization of MMA by ESR. We observed a distinct difference in propagating radical concentration profiles at high conversion in various particle size MMA batch emulsion polymerizations. The faster radical termination observed by ESR in the larger particle size polymerizations could be explained by inhomogeneous distribution of the propagating radicals. Although the overall propagating radical concentration based on total polymer volume for various particle sizes is comparable, such an inhomogeneity would cause a higher local radical concentration in the outermost layer of larger particles. This higher local concentration would result in a higher overall rate of termination by the short radicals entering from the aqueous phase and by residual termination from propagation with remaining monomer.

In addition to effects on the propagating free-radical concentrations, we have found that the particle size has a significant effect on the polymerization kinetics and on the polymer molecular weight and the molecular weight distribution. Details of the study of molecular weight and molecular weight distribution will be presented in a separate report.[30]

Acknowledgment. We thank Willie Lau, Cheryl Whitehead, Susan Fitzwater, and Lily Xie of Rohm and Haas for contributions to this work and Rohm and Haas Co. for support and permission to publish this work. We also thank Prof. Bob Gilbert for many stimulating discussions, and the reviewers for a number of useful comments.

Glossary

A_s	total surface area of all the particles in the reactor, nm^2
D_{diff}	diffusion coefficient of MMA, cm^2/s
D_{final}	diameter of particle at 100% conversion, nm
D_t	diameter of particle at time t, nm
k_p	propagation rate coefficient, L/mol·s
[M]	total monomer concentation, mol/L
$[M]_p$	monomer concentration in the particles, mol/L
$\bar{n}$	average number of radicals per particle
N_A	Avogadro's number
N_p	total number of particles
ρ_p	polymer density, g/cm^3
[R•]	radical concentration based on emulsion volume, mol/L
$[R•]_p$	radical concentration in the particles, mol/L
$\Delta[R•]_p$	relative decrease in radical concentration based on the maximum radical concentration
r	distance, cm
t	time, s
V_E	total emulsion volume of the reaction, L
$\bar{V}_{R•}$	average volume each radical occupies, nm^3
$\bar{V}_{R•,inhomo}$	average volume each radical occupies assuming all radicals are located in the outer 40-nm layer in the particle, nm^3
w_p	polymer weight fraction in total monomer polymer mix
w_p^d	polymer fraction in the particles when $[R•]_p$ starts to decay
W_t	polymer weight at time t, g
W_{final}	total polymer weight at 100% conversion, g
W_{seed}	weight of the seed polymer, g
x	conversion

References and Notes

(1) James, H. L.; Piirma, I. In *Emulsion Polymerization*; Piirma, I., Gardon, J. L., Eds.; American Chemical Society: Washington, DC, 1976; pp 197−209.
(2) Fontenot, K.; Schork, F. J. *J. Appl. Polym. Sci.* **1993**, *49*, 633.
(3) Yu, Z.; Li, B.; Cai, M; Li, B.; Cao, K. *J. Appl. Polym. Sci.* **1995**, *55*, 1209.
(4) Adams, M. E.; Russell, G. T.; Casey, B. S.; Gilbert, R. G.; Napper, D. H. *Macromolecules* **1990**, *23*, 4624.
(5) Russell, G. T.; Gilbert, R. G.; Napper, D. H. *Macromolecules* **1992**, *25*, 2459.
(6) Russell, G. T.; Gilbert, R. G.; Napper, D. H. *Macromolecules* **1993**, *26*, 3538.
(7) Tian, Y.; Wang, G.-B.; Shen, J.-C.; Zheng, Y.-G.; Qiu, Z.-W. *Chin. Sci. Bull. (Engl. Ed.)* **1989**, *34*, 396.
(8) Faldi, A.; Tirrell, M.; Lodge, T. P. *Macromolecules* **1994**, *27*, 4176.
(9) Mills, M. F.; Gilbert, R. G.; Napper, D. H. *Macromolecules* **1990**, *23*, 4247.
(10) Mills, M. F.; Gilbert, R. G.; Napper, D. H.; Rennie, A. R.; Ottewill, R. H. *Macromolecules* **1993**, *26*, 3553.
(11) Croxton, C. A.; Mills, M. F.; Gilbert, R. G.; Napper, D. H. *Macromolecules* **1993**, *26*, 3563.
(12) Yang, S.-I.; Klein, A.; Sperling, L. H.; Casassa, E. F. *Macromolecules* **1990**, *23*, 4582.
(13) Gilbert, R. G. *Emulsion Polymerization: A Mechanistic Approach*; Academic: London, 1995.
(14) Gilbert, R. G. *Trends Polym. Sci.* **1995**, *3*, 222.
(15) Bresler, S. E.; Nazbekov, E. N.; Formichev, V. N.; Shadrin, V. N. *Makromol. Chem.* **1972**, *157*, 167.
(16) Bresler, S. E.; Nazbekov, E. N.; Shadrin, V. N. *Makromol. Chem.* **1974**, *175*, 2875.
(17) Tian, Y.; Wang, G.-B.; Shen, J.-C.; Zheng, Y.-G.; Qiu, Z.-W. *Chin. Sci. Bull. (Engl. Ed.)* **1989**, *34*, 396.
(18) Carswell, T. G.; Hill, D. J. T.; Hunter, D. S.; Pomery, P. J.; O'Donnell, J. H.; Winzor, C. L. *Eur. Polym. J.* **1990**, *26*, 541.
(19) Shen, J.-C.; Tian, Y.; Wang, G.-B.; Yang, M.-L. *Sci. China (Ser. B)* **1990**, *33*, 1040.
(20) Zhu, S.; Tian, Y.; Hamielec, A. E.; Eaton, D. R. *Macromolecules* **1990**, *23*, 1144.
(21) Shen, J.-C.; Wang, G.-B.; Yang, M.-L.; Zheng, Y.-G. *Polym. Int.* **1992**, *28*, 75.
(22) Ballard, M. J.; Gilbert, R. G.; Napper, D. H.; Pomery, P. J.; O'Donnell, J. H. *Macromolecules* **1984**, *17*, 504.
(23) Ballard, M. J.; Gilbert, R. G.; Napper, D. H.; Pomery, P. J.; O'Sullivan, P. W.; O'Donnell, J. H. *Macromolecules* **1986**, *19*, 1303.
(24) Lau, W.; Westmoreland, D. G.; Novak, R. W. *Macromolecules* **1987**, *20*, 457.
(25) Westmoreland, D. G.; Lau, W. *Macromolecules* **1989**, *22*, 496.
(26) Cutting, G. R.; Tabner, B. J. *Macromolecules* **1993**, *26*, 951.
(27) Lau, W.; Westmoreland, D. G. *Macromolecules* **1992**, *25*, 4448.
(28) Chang, H.-R.; Parker, H.-Y.; Westmoreland, D. G. *Macromolecules* **1992**, *25*, 5557.
(29) Xie, L. Q. *Polymer* **1993**, *34*, 4579.
(30) Westmoreland, D. G.; Chang, H.-R.; Parker, H.-Y., manuscript in preparation.
(31) Ballard, M. J.; Napper, D. H.; Gilbert, R. G. *J. Polym. Sci., Polym. Chem. Edn.* **1984**, *22*, 3225.
(32) Maxwell, I. A.; Morison, B. R.; Napper, D. H.; Gilbert, R. G. *Macromolecules* **1991**, *24*, 1629.
(33) Tian, Y.; Zhu, S.; Hamielec, A. E.; Fulton, D. B.; Eaton, D. R. *Polymer* **1992**, *33*, 384.
(34) Tonge, M. P.; Pace, R. J.; Gilbert, R. *Macromol. Chem. Phys.* **1994**, *195*, 3159.
(35) In these calculations no correction was made for monomer present in the aqueous phase.
(36) Russell, G. T.; Gilbert, R. G.; Napper, D. H. *Macromolecules* **1988**, *21*, 2133.
(37) Fitzwater, S. J.; Chang, H.-R.; Parker, H.-Y.; Westmoreland, D. G., manuscript in preparation.

MA951652O